Viscoelasticity and Stokes-Einstein relation in repulsive and attractive colloidal glasses

Antonio M. Puertas
Group of Complex Fluid Physics, Departamento de Física Aplicada, Universidad de Almería, 04120 Almeria, Andalucía, Spain

Cristiano De Michele and Francesco Sciortino
Dipartimento di Fisica, Intstituto Nazionale per la Fisica della Materia, Università di Roma La Sapienza, Piazzale Aldo Moro 2, I-00185 Roma, Italy and CNR-INFM-SOFT, Università di Roma La Sapienza, Piazzale Aldo Moro 2, I-00185 Roma, Italy

Piero Tartaglia
Dipartimento di Fisica, Intstituto Nazionale per la Fisica della Materia, Università di Roma La Sapienza, Piazzale Aldo Moro 2, I-00185 Roma, Italy and CNR-INFM-SMC, Università di Roma La Sapienza, Piazzale Aldo Moro 2, I-00185 Roma, Italy

Emanuela Zaccarelli
Dipartimento di Fisica, Intstituto Nazionale per la Fisica della Materia, Università di Roma La Sapienza, Piazzale Aldo Moro 2, I-00185 Roma, Italy and CNR-INFM-SOFT, Università di Roma La Sapienza, Piazzale Aldo Moro 2, I-00185 Roma, Italy

(Received 21 May 2007; accepted 25 July 2007; published online 9 October 2007)

We report a numerical investigation of the viscoelastic behavior in models for steric repulsive and short-ranged attractive colloidal suspensions, along different paths in the attraction strength vs packing fraction plane. More specifically, we study the behavior of the viscosity (and its frequency dependence) on approaching the repulsive glass, the attractive glass, and in the reentrant region where viscosity shows a nonmonotonic behavior on increasing attraction strength. On approaching the glass lines, the increase of the viscosity is consistent with a power-law divergence with the same exponent and critical packing fraction previously obtained for the divergence of the density fluctuations. Based on mode-coupling calculations, we associate the increase of the viscosity with specific contributions from different length scales. We also show that the results are independent of the microscopic dynamics by comparing Newtonian and Brownian simulations for the same model. Finally, we evaluate the Stokes-Einstein relation approaching both glass transitions, finding a clear breakdown which is particularly strong for the case of the attractive glass. © *2007 American Institute of Physics*. [DOI: 10.1063/1.2772628]

I. INTRODUCTION

Understanding dynamic arrest in colloidal system is crucial in disparate technological applications (e.g., food industry,[1] biomaterials,[2] painting). Development of basic science also requires a deeper understanding of the different routes and mechanisms leading to dynamic arrest (glasses and gels).[3–6] In this respect, model colloidal systems are playing a very important role due to their versatility. It is indeed possible to tailor the shape, size, and structure of the colloidal particles, making it possible to design specific colloidal interaction potentials.[7] Furthermore, accurate experimental methods are now available for investigating the structure and the dynamics of colloids even at the single particle level.[8] Unexpected novel behaviors regarding the glass transition have been theoretically predicted[9–13] and experimentally observed[14–19] in the cases in which colloidal particles interact, beside the hard core, via a short-ranged attractive interaction potentials (when the attraction range is about one-tenth of the particle diameter or less). The predictions based on application of the ideal mode coupling theory[20] (MCT) for supercooled liquids suggest that the standard packing-driven hard-sphere glass transition transforms—discontinuously in some cases—into a novel type of glass transition driven by the short-range attraction. The competition between the two different arrest mechanisms introduces slow-dynamics features which are not commonly observed in molecular and atomic systems. Experiments on solutions of (hard-sphere-like) colloidal particles [either poly(methyl methacrylate) or polystyrene micronetwork spheres] in the presence of small nonadsorbing polymers[14,15,17] have shown that there exists a window of polymer densities in which the mobility of the colloidal particles has a maximum for a finite value of polymer concentration. Moreover, for small and large polymer concentrations, the strength of the α relaxation (the non-ergodicity parameter) is found to be very different, suggesting that indeed the viscoelastic response of the repulsive and attractive glasses will also be significantly different. Molecular dynamics simulations of short-ranged models[21–24] have confirmed the picture resulting from the theoretical predictions and validated by the experiments. A recent review can help summarizing the experimental and numerical studies in short-ranged attractive colloids.[5]

The numerical results have been so far mostly limited to

the study of self and collective properties of the density fluctuations. Despite the strong link with experiments and the relevance to industrial applications, the numerical evaluations of the viscosity η and viscoelastic properties $\tilde{\eta}(\omega)$ have lagged behind, since significant computational effort is requested for accurate calculation of $\tilde{\eta}(\omega)$, even more for states close to dynamical arrest. Experimentally, measurements of η close to the repulsive hard-sphere glass transition show an apparent divergence, but there is no consensus on the functional form describing such increase.[25,26] For colloidal gels, a power-law divergence has been reported in connection to the gel transition.[27] Theoretically, MCT predicts an asymptotic power-law divergence, with identical exponent, of all dynamical quantities with the distance from the transition, and hence η, the time scale of the density fluctuations τ, and the inverse of the self-diffusion coefficient $1/D_0$ should diverge with the same critical parameters.

In this article, we attempt a characterization of the viscoelastic properties of two different short-ranged attractive potentials (a polydisperse Asakura-Osawa and a square well) along three different paths in the attraction strength-packing fraction plane, which allow us to access both the repulsion driven and attraction driven glass transitions with both systems. We show the divergence of the viscosity, as well as the diffusion coefficient or structural relaxation time, as the repulsive and attractive glasses are approached. At high density, the isochoric path shows the reentrant glass; the viscosity increases about three orders of magnitude upon either increasing or decreasing the strength of attraction.

The article is organized as follows. In Sec. II we introduce the numerical models and describe the methods to calculate the viscosity. In Sec. III we describe the paths investigated and provide some background information on the behavior of the diffusion and collective density fluctuations along these paths. In Sec. IV we discuss the observed behavior of the viscosity on approaching the repulsive and the attractive glass lines. In Sec. V, guided by theoretical MCT predictions for the viscosity, we provide evidence that the viscoelastic behavior close to the two different glass lines is controlled by density fluctuations of different wavelengths. Finally in Sec. VI we report a study of the density and attraction strength dependence of the Stokes-Einstein relation.

II. NUMERICAL SIMULATIONS

A. Model A: Square well and hard-sphere binary mixture

We perform molecular dynamics (MD) simulations of a 50:50 binary mixture of 700 particles of mass m with diameters $\sigma_{AA}=1.2$ and $\sigma_{BB}=1$ (setting the unit of length). The particles interact through a hard core repulsion complemented by a narrow square well (SW) pair potential. The hard core repulsion for the AB interaction occurs at a distance $\sigma_{AB}=(\sigma_{AA}+\sigma_{BB})/2$. The SW potential is

$$V_{\mathrm{SW}}(r)=\begin{cases}\infty, & r<\sigma_{ij}\\ -u_0, & \sigma_{ij}<r<\sigma_{ij}+\Delta_{ij}\\ 0, & r>\sigma_{ij}+\Delta_{ij},\end{cases} \tag{1}$$

where r is the distance between particles of types $i,j=A,B$, the depth of the well u_0 is set to 1, and the widths Δ_{ij} are such that $\Delta_{ij}/(\sigma_{ij}+\Delta_{ij})=0.03$. Temperature T is measured in units of u_0 ($k_B=1$), the attraction strength $\Gamma=1/T$, and time t in $\sigma_{BB}(m/u_0)^{1/2}$. The use of a binary mixture allows us to suppress crystallization at high packing fraction $\phi_c=(\rho_A\sigma_A^3+\rho_B\sigma_B^3)\pi/6$, where $\rho_i=N_i/L^3$, L being the box size, and N_i the number of particles for each species. The system undergoes phase separation into a gas and a liquid for large attraction strength in a wide range of packing fractions:[28] The critical point is located roughly at $\Gamma_c\approx 3.33$ and $\phi_c\approx 0.27$ (the latter is estimated from the Noro-Frenkel scaling[29] invariance close to the Baxter limit[30]). Previous studies[23,28,31] of the same model allowed us to locate the dynamical arrest line and the spinodal curve. The "numerical" glass line was determined by extrapolation via a power-law fitting of the normalized diffusion coefficient D/D_0, i.e., $D/D_0\sim|\phi_c-\phi_c^G|^\gamma$,[31] where $D_0=\Gamma^{1/2}$. This study was complemented by the calculation of the MCT glass lines for the same model. Hence, a bilinear transformation of ϕ_c and T was used to superimpose the theoretical onto the numerical glass line.

We also study, as discussed below, the same 50:50 binary mixture of 700 particles, with the same σ_{AA}, σ_{BB}, and σ_{AB} above, but interacting simply as hard spheres, for which the potential reads

$$V_{\mathrm{HS}}(r)=\begin{cases}\infty, & r<\sigma_{ij}\\ 0, & r>\sigma_{ij}.\end{cases} \tag{2}$$

For Newtonian dynamics simulations, we used a standard event-driven (ED) algorithm.[32] We also perform Brownian dynamics (BD) simulations of the same model to ensure the independence of the viscoelastic calculations of the microscopic dynamics. For BD simulations we exploit a recently developed[33] BD algorithm, which we shortly describe below. For a more extensive discussion we invite the reader to consult Ref. 34.

If the position Langevin equation is considered, i.e.,

$$\dot{\mathbf{r}}_i(t)=\frac{D_0}{k_BT}\mathbf{f}_i(t)+\mathring{\mathbf{r}}_i(t), \tag{3}$$

where $\mathbf{r}_i(t)$ is the position of particle i, D_0 is the short-time (bare) diffusion coefficient, $\mathbf{f}_i(t)$ is the total force acting on the particle, and $\mathring{\mathbf{r}}_i(t)$ a random thermal noise satisfying $\langle\mathring{\mathbf{r}}_i(t)\cdot\mathring{\mathbf{r}}_i(0)\rangle=6D_0\delta(t)$. The BD integration scheme of Eq. (3) can be schematized as follow: (i) every $t_n=n\Delta t$ (n integer) extract velocities $\mathbf{v}_i$ according to a Maxwellian distribution of variance $\sqrt{k_BT/m}$; (ii) evolve the system between t_n and $t_n+\Delta t$ according to the laws of ballistic motion (performing standard ED molecular dynamics).

The present binary mixture model allows us to study the viscoelastic properties within the reentrant liquid region enclosed by the nearby attractive and repulsive glass transitions. On the other hand, due to phase separation, it does not allow us to approach the attractive glass line at moderate

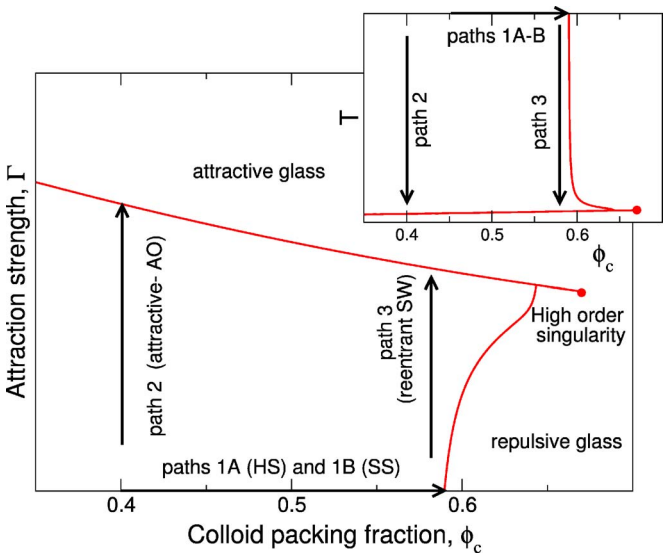

FIG. 1. Schematic phase diagram showing the attraction and repulsion driven glasses and the three paths followed in this work. Note that path 1 (infinite temperature limit) is studied within both models. The inset shows the three paths in the temperature-packing fraction representation.

density. Hence we will study V_{HS} for varying ϕ_c (path 1A in Fig. 1) and V_{SW} at fixed $\phi_c=0.58$ on varying T (path 3 in Fig. 1).

B. Model B: Asakura-Oosawa polydisperse system

We also study an interaction potential based on the Asakura-Oosawa model to make a direct link with experiments in colloid-polymer mixtures. A polydisperse system, comprised of 1000 particles, is simulated with the standard velocity Verlet algorithm for Newtonian dynamics in the canonical ensemble, which requires a continuous differentiable potential. To this end, a soft core was used instead of the hard core in model A,

$$V_{\mathrm{sc}}(r) = (\sigma_{ij}/r)^{36}, \tag{4}$$

where $\sigma_{ij}=(\sigma_i+\sigma_j)/2$, with σ_i the diameter of particle i. Diameters were distributed according to the flat distribution $[\sigma-\delta,\sigma+\delta]$ with σ the mean diameter and $\delta=0.1\sigma$. The short-range attraction between particles is given by the Asakura-Oosawa model for polydisperse systems,

$$V_{\mathrm{AO}}(r) = -k_BT\phi_p\left\{\left[(\bar{\eta}+1)^3 - \frac{3r}{2\xi}(\bar{\eta}+1)^2 + \frac{r^3}{2\xi^3}\right] + \frac{3\xi}{8r}(\eta_1-\eta_2)^2\left[(\bar{\eta}+1) - \frac{r}{\xi}\right]^2\right\}, \tag{5}$$

for $\sigma_{12}\leqslant r\leqslant\sigma_{12}+\xi$) and 0 for larger distances; $\eta_i=\sigma_i/\xi$, $\bar{\eta}=(\eta_1+\eta_2)/2$, and ϕ_p is the volume fraction of the polymer. The range of the interaction, ξ, is the polymer size, and its strength is proportional to ϕ_p, the concentration of ideal polymers. To ensure that the interaction potential $V_{\mathrm{sc}}+V_{\mathrm{AO}}$ has its minimum at σ_{12}; the Asakura-Oosawa potential is connected analytically to a parabola at $\sigma_{12}+\xi/10$.[35] For average particles, $\sigma_1=\sigma_2=\sigma$, the attraction strength of the Asakura-Oosawa potential is given by $V_{\mathrm{min}}=-k_BT\phi_p(3/2\eta+1)$, which for $\xi=0.1$ is $V_{\mathrm{min}}=-16k_BT\phi_p$.

Because the attractive glass transition occurs inside the liquid-gas spinodal, it cannot be accessed directly from the fluid with this potential. Thus, we have added a long range repulsive barrier to the interaction potential that destabilizes a macroscopic separation into two fluid phases. The barrier is given by

$$V_{\mathrm{bar}}(r) = k_BT\left\{\left(\frac{r-r_1}{r_0-r_1}\right)^4 - 2\left(\frac{r-r_1}{r_0-r_1}\right)^2 + 1\right\}, \tag{6}$$

for $r_0\leqslant r\leqslant r_2$ and zero otherwise, with $r_1=(r_2+r_0)/2$. The limits of the barrier were set to $r_0=\sigma_{12}+\xi$ and $r_2=2\sigma$, and its height is $1k_BT$. The barrier raises the energy of a dense phase, so that liquid-gas separation is suppressed. The resulting total interaction,

$$V_{\mathrm{tot}}(r) = V_{\mathrm{sc}}(t) + V_{\mathrm{AO}}(r) + V_{\mathrm{bar}}(r), \tag{7}$$

is analytical everywhere and allows straightforward integration of the equations of motion.

This model allows us to study the viscoelastic properties of the fluid close to the attraction driven glass transition at moderate density, i.e., far from the high order singularity. We will use this system to approach the repulsive glass with increasing ϕ_c at $\phi_p=0$, hence using simply V_{sc} (path 1B in Fig. 1), as well as to study the attractive glass at moderate density $\phi_c=0.40$ (path 2 in Fig. 1) by using V_{tot}.

C. Computation of viscosity

The shear viscosity η is given by the Green-Kubo relation,

$$\eta \equiv \int_0^\infty dt C_{\sigma\sigma}(t) = \frac{\beta}{3V}\int_0^\infty dt \sum_{\alpha<\beta}\langle\sigma^{\alpha\beta}(t)\sigma^{\alpha\beta}(0)\rangle, \tag{8}$$

which expresses η as the integral of the correlation function of the nondiagonal terms of the microscopic stress tensor, $\sigma^{\alpha\beta}=\Sigma_{i=1}^N mv_{i\alpha}v_{i\beta}-\Sigma_{i<j}^N(r_{ij\alpha}r_{ij\beta}/r_{ij})V'(r_{ij})$, where V is the volume of the simulation box, $v_{i\alpha}$ is the αth component of the velocity of particle i, and V' is the derivative of the total potential. $\langle\cdots\rangle$ indicates an average over initial conditions. However, from the computational point of view, it is more convenient to use the Einstein relation,

$$\eta = \lim_{t\to\infty}\eta(t) = \frac{\beta}{6V}\lim_{t\to\infty}\frac{1}{t}\langle\Delta A(t)^2\rangle, \tag{9}$$

where $A(t)$ is the integral from 0 to t of the three off-diagonal terms of the stress tensor,

$$\Delta A(t) = A(s+t) - A(s) = \int_s^{s+t}\sum_{\alpha<\beta}\sigma^{\alpha\beta}(s')ds'. \tag{10}$$

Using Eq. (9) is analogous to the calculation of the diffusion coefficient as the long time slope of the mean squared displacement.

For discontinuous potentials (hard cores or square wells), Eq. (9) can still be used[36] despite the impulsive character of the interactions. In this case,

TABLE I. Glass transition point ϕ_c^G, von Schweidler exponent b, and divergence exponents of the characteristic time of the decay of density fluctuations γ_τ and of the diffusion coefficient γ_D for models A and B in the absence of attraction, i.e., respectively, V_{HS} and V_{sc}, along path 1.

	ϕ_c^G	b	γ_τ	γ_D
Model A: V_{HS}	0.584	0.51	2.75	2.17
Model B: V_{sc}	0.594	0.53	2.72	2.02

$$[\Delta A(t)]_{\mathrm{HS,SW}} = \sum_{\text{collisions}} \sum_{\alpha\neq\beta} \left[\left(m \sum_{i=1}^{N} v_{i\alpha} v_{i\beta} \right) \tau_t + m(x_{k\alpha} - x_{l\alpha})(v_{k\beta}^{\text{after}} - v_{l\beta}^{\text{before}}) \right], \tag{11}$$

where τ_t is the time elapsed from the previous collision, k and l are the two colliding particles, $x_{k\alpha}$ is the position of particle k in direction α, and $(v_{k\beta}^{\text{after}} - v_{l\beta}^{\text{before}})$ is the momentum change in direction β of particle k due to the collision with particle l. We have not attempted to numerically recover $C_{\sigma\sigma}(t)$ from $\Delta A(t)$.

D. Units

For both studied models we report states in the packing fraction versus attraction strength plane $(\phi_c - \Gamma)$. For model A, the attraction strength is given by the inverse temperature (for HS temperature is irrelevant and is set equal to 1), whereas for model B, $\Gamma = -V_{\mathrm{min}}$. Distances are measured using σ_{BB} for model A and the mean diameter σ for model B, while the particle mass m is always set to 1. The stress correlation function is measured in units of $k_B T/\sigma^3$, and time in units of $(\sigma^2 m/k_B T)^{1/2}$. The viscosity is thus given in $(mk_B T)^{1/2}/\sigma^2$. For the integration of the equations of motion in model B, the time step was set to $\delta t = 0.0025/\sqrt{3}$.

III. DESCRIPTION OF PATHS, TRANSITION, FITS, EXPONENTS

Using the models presented above, we numerically study the following paths schematized in Fig. 1.

Path 1. The zero-attraction case for both models, i.e., the hard and the soft sphere models. The two models are not identical along this path because (i) the Asakura-Oosawa model has a soft repulsion (although the r^{-36} core is quite hard and no important effects are expected[37]) and more importantly (ii) the size distributions are different: bimodal in model A versus continuous in model B. Model B has been studied previously along this path monitoring the self-diffusion and the density correlation functions.[38] The glass transition points and the exponents controlling the power-law divergence of the structural relaxation time scale γ_τ and the diffusion coefficient γ_D, as well as the von Schweidler exponent b (which provides a measure of the slow decay of the density correlation function), are shown in Table I for both systems. The difference in the critical packing fractions can be attributed to the different size distributions of the two models. The exponents γ_τ and γ_D, on the other hand, are very similar in both models.

TABLE II. Glass transition point γ^G, von Schweidler exponent b, and divergence exponents γ_τ and γ_D for models A and B in the presence of attraction, i.e., respectively, V_{SW} and V_{tot}, respectively, along path 3 and 2.

	Γ^G	b	γ_τ	γ_D
Path 2: V_{tot}	9.099	0.37	3.23	1.23
Path 3: V_{SW}	3.56	0.33	3.75	2.2

Path 2. Approaching the attractive glass. This path is studied with model B, for which the liquid-gas transition is destabilized and the glass transition can be approached from the fluid. This path has been studied previously monitoring the density correlation functions[35,39] and the viscosity,[40] and the glass transition is found for $\Gamma^G = 9.099$; the associated von Schweidler and critical exponents are given in Table II.

Path 3. The reentrant region and the approach to the attractive glass. This path is studied with model A at $\phi_c = 0.58$, a value well within the reentrant region.[23] The corresponding parameters for this path are provided in Table II. At large temperature, the glass transition is approached but not reached because the studied packing fraction is close, but smaller than ϕ_c^G for V_{HS}, i.e., the path is parallel to the repulsive glass line in the limit $T \to \infty$.

Note that, as predicted from MCT, the attractive glass shows lower von Schweidler exponents than the repulsive glass, for both paths and models, while γ_τ is larger. This implies that the divergence of the time scale for structural relaxation is more abrupt. For the square well mixture, quantitative results from simulations and MCT are available,[31] predicting the transition point at $\phi_c = 0.58$ for $\Gamma^{G,\mathrm{MCT}} \simeq 3.70$, in quite good agreement with that estimated from the fits $\Gamma^G \simeq 3.56$. For path 2 a quantitative comparison with MCT has been also recently performed,[41] showing that the driving mechanism for the slowing down observed in the simulation is driven by the short-range attractions [large-q modes of $S(q)$].

IV. VISCOSITY RESULTS

In this section we study the viscosity along the three paths described above.

A. Hard and soft spheres: Paths 1A and 1B

In Fig. 2 we present, along path 1*B*, the stress correlation function for V_{sc} at different concentrations (upper panel) and the integral of the squared nondiagonal terms of the stress tensor (lower panel). The correlation functions have been averaged over 5000 independent calculations. Note the progressive development of a two-step decay in $C_{\sigma\sigma}(t)$ as the concentration increases and the glass transition is approached, with the second (structural) decay of $C_{\sigma\sigma}(t)$ moving to longer and longer times. This implies that stress relaxes slower and slower, or equivalently that the system increases its ability to store the stress; i.e., the system becomes viscoelastic. Additionally, it can be observed that $C_{\sigma\sigma}(0)$ grows close to the transition. Both effects are responsible for the increase of the viscosity upon increasing the

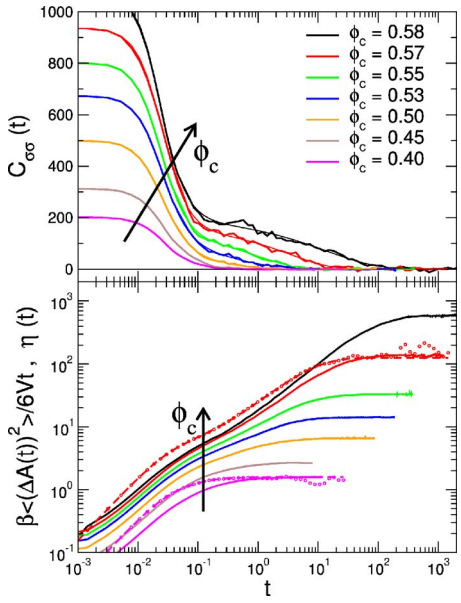

FIG. 2. Upper panel: Stress correlation function $C_{\sigma\sigma}(t)$ for V_{sc}. The thin lines are empirical fittings to describe the data (see Sec. V for details). Lower panel: Full lines are $\beta\langle(\Delta A(t))^2\rangle/6Vt$ [from the Einstein relation, Eq. (9)] for all studied ϕ_c. For two specific values of ϕ_c (ϕ_c=0.57 and ϕ_c=0.40) we also show $\eta(t)$ obtained using a direct integration of $C_{\sigma\sigma}(t)$ (symbols), and integration of the fitting curves (dashed thick). Note that while $\eta(t)$ and $\beta(\Delta A(t))^2/6Vt$ have the same long time value, their time dependence is different.

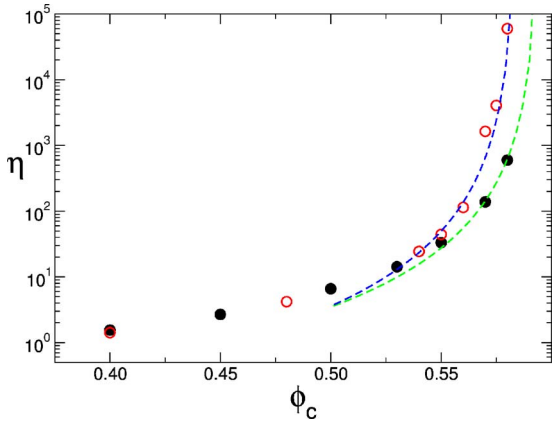

FIG. 3. Viscosity of soft (full black circles) and hard (empty red circles) spheres as a function of particle packing fraction, approaching the glass transition. Lines are power-law fits to points with $\phi_c > 0.50$. The values of the critical packing fraction have been fixed to the previously determined values (see Table I), i.e., ϕ_c^G=0.594 and ϕ_c^G=0.584 for soft and hard spheres, respectively. The corresponding fitting exponents γ_η are 2.74 and 2.9.

packing fraction, but the increase in the time scale is the one providing the leading contribution to the integral [see Eq. (8)].

The integral of the stress correlation function is very noisy, and the numerical evaluation of the viscosity is more accurate if calculated using the Einstein relation [Eq. (9)], as shown in the lower panel of Fig. 2. For comparison, the integral of the functional form used to describe $C_{\sigma\sigma}(t)$ (see below) is also included for two state points. Note that all three quantities show the same long time limit, i.e., the viscosity does not depend on the way it is calculated. At intermediate times, the integral of $C_{\sigma\sigma}(t)$ and its fitting are in perfect agreement, but the integral of the fitted function is less noisy. Thus, we will calculate viscosities using the Einstein relation in Eq. (9).

The viscosity, as given by the long time plateau, grows with increasing particle density, as shown in Fig. 3. This increase is consistent with a power law, diverging at the transition point estimated from the structural relaxation time and from the diffusion coefficient ϕ_c^G=0.594.[40] The exponent for this power law γ_η=2.74 is similar to γ_τ but different from γ_D, as reported in Table I.

For hard spheres, path 1A, the viscosity can only be calculated by integrating the squared nondiagonal terms obtained from Eq. (11). For these calculations, $\langle(\Delta A(t))^2\rangle$ was averaged over 20 independent starting configurations and over time for a minimum of $70\tau_\alpha$, where τ_α is the density relaxation time at the wavelength corresponding to the nearest-neighbor peak. The behavior of $\langle(\Delta A(t))^2\rangle$ along this path (not shown) is very similar to that reported in Fig. 2 for model B, and the viscosity, included in Fig. 3, increases as the glass transition is approached. A power-law divergence with exponent $\gamma_\eta \simeq 2.9$ is observed for the viscosity, with the transition point at ϕ_c^G=0.584, slightly lower than for V_{sc}. The value of the exponent is, again, in good agreement with γ_τ but quite different from γ_D.

B. Attractive glass: Path 2

In this section, we analyze the viscoelastic behavior close to the attractive glass. As discussed above, for this purpose we use model B for which the liquid-gas separation is suppressed by the presence of the added repulsive barrier, allowing for the study of low density (ϕ_c=0.40) in a homogeneous system. The attraction between particles induces a minimum after the short time (microscopic) relaxation in the stress correlation function (not shown), which introduces a negative correlation at intermediate attraction strengths.[40] At high attraction strength, the correlation is positive at all times, and after the minimum, $C_{\sigma\sigma}(t)$ shows the development of a slow decay and a large increase of the value at zero time $C_{\sigma\sigma}(0)$, similarly to the phenomenology observed for the repulsive glass. This indicates that the system is becoming solidlike due to the bonds formed in the system.

$\langle(\Delta A(t))^2\rangle$, used to calculate the viscosity, grows dramatically upon increasing the attraction strength. The long time limit value η is shown in Fig. 4 as a function of attraction strength. The data can be fitted using a power-law divergence as a function of the distance from the transition $\Gamma - \Gamma^G$, where Γ^G is reported in Table II. The exponent γ_η=3.16 is again in good agreement with γ_τ.

C. Reentrance region: Path 3

Path 3 is a high density isochoric path, where the attractive and repulsive glass lines are about to merge. Varying the attraction strength, the system can be studied in states close to the repulsive or to the attractive glass. This path is studied only with system A because the short interaction range of the studied SW opens up a large fluid region between the two glasses.

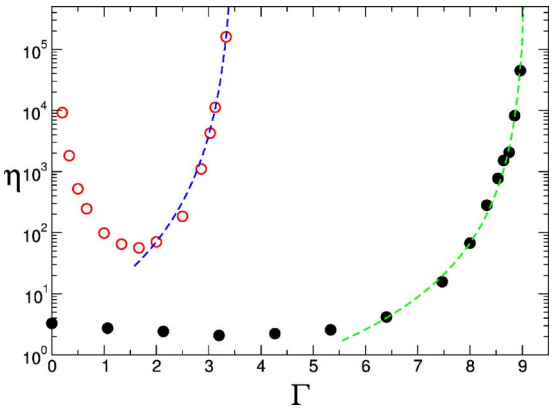

FIG. 4. Viscosity approaching the attractive glass transition along path 2 (full black circles), and in the reentrant region along path 3 (empty red circles), as a function of attraction strength. The lines represent power-law fittings (with values of the critical attraction strength fixed to the previously determined values reported in Table II), with exponents γ_η equal to 3.16 for path 2 and 3.75 for the attractive side of the reentrant path 3.

Figure 5 shows $\langle(\Delta A(t))^2\rangle/t$ calculated using Eq. (11). The corresponding viscosity is reported in Fig. 4 as a function of Γ. As expected in this region, the viscosity increases both at low temperature due to the proximity of the attractive glass and at high temperature because of the nearby repulsive glass. A power-law divergence describes the attractive glass increase of η with exponent $\gamma_\eta \simeq 3.75$, i.e., the same that is found also for the density relaxation time γ_τ. Data refer to an average over 20 independent starting configurations and over time for a minimum of $200\tau_\alpha$. A pronounced reentrant behavior, covering two full decades toward both limits, is observed in η, similar to that reported previously for the diffusion coefficient D in the same system.[23]

V. COMPARISON OF $C_{\sigma\sigma}(t)$ WITH MODE COUPLING THEORY

MCT predicts[42] that the stress correlation function is related to an integral over all wave vectors of the density correlation functions,

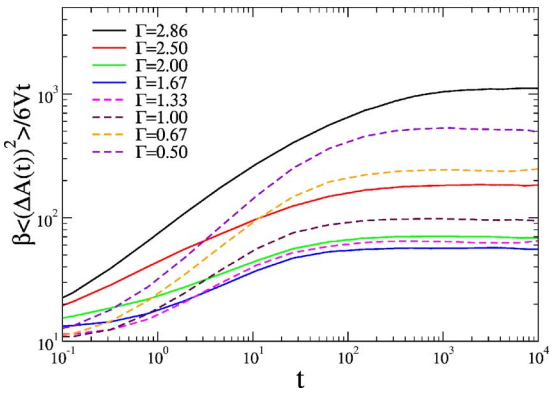

FIG. 5. $\beta\langle(\Delta A(t))^2\rangle/6Vt$ for different attraction strengths Γ along the isochore $\phi_c=0.58$ for path 3A. On decreasing Γ, the long time limit first decreases (full lines) and then increases again (dashed lines), resulting in a pronounced reentrant behavior of the viscosity.

$$C_{\sigma\sigma}(t) = \frac{k_B T}{60\pi^2}\int_0^\infty dq q^4 \left[\frac{d\ln S(q)}{dq}\Phi_q(t)\right]^2. \tag{12}$$

We theoretically calculate $C_{\sigma\sigma}(t)$ along two paths analogous to paths 1B and 2 studied in simulations to compare the full time behavior of the stress correlation function. Hence, we study (i) A one-component hard-sphere system with increasing ϕ_c, using the Percus-Yevick (PY) structure factor as input; (ii) a one-component Asakura-Oosawa (AO) model with size ratio $\xi=0.1$ at fixed packing fraction $\phi_c=0.40$. Here $S(q)$ is calculated using PY closure for the two-component Asakura-Oosawa mixture. This model mixture is composed of HS colloidal particles and ideal-gas polymers with HS interactions between polymers and colloids.[43] The obtained colloid-colloid structure factor is used as input to a one-component MCT, a treatment based on the validity of an effective one-component description for small polymer-colloid size ratio.[44,45] We did not use the fundamental measure density functional theory[46,47] which yields analytical expressions for $S_{ij}(k)$ as done previously[48] because within this closure the system shows spinodal instability before MCT would actually give a glass. This is not the case with PY closure, for which only a very tiny increase in the structure factor at small q is found approaching the MCT transition.

We solved the full dynamical MCT equations, as well as their long time limit, to calculate the viscoelastic properties close to the glass transition. Our calculations are based on standard algorithms already developed some years ago[49] and we use a grid of 1500 wave vectors with mesh $\Delta q=0.314$.

The long time limit of the integrand of Eq. (12),

$$I(q) = \lim_{t\to\infty} q^4\left[\frac{d\ln S(q)}{dq}\Phi_q(t)\right]^2 = q^4\left[\frac{d\ln S(q)}{dq}f_q^c\right]^2, \tag{13}$$

is plotted as a function of $q\sigma$, in Fig. 6 for both studied systems, f_q^c being the critical nonergodicity parameter at the MCT transition. The same figure reports also f_q^c and the input static structure factor, also at the transition, $S^c(q)$.

For the repulsive glass we find that the dominant contribution to the integral is provided by the wave-vector region around the nearest-neighbor peak, i.e., $q^*\sigma \approx 6.5$. For the attractive glass, on the other hand, the dominant contribution is found at much larger q values, i.e., $q^*\sigma \approx 24$ [in the region of the fourth peak of $S(q)$], providing another confirmation of the importance of small length scales in the localization properties of such a glass.[4] Moreover, in this case, the integrand is not just peaked around a specific value, but it is rather spread within a very large q interval. The amplitude of the integrand is also much larger in the case of the attractive glass as compared to the repulsive glass.

We can then compare in the upper panel of Fig. 7 the theoretical stress correlation function with the squared theoretical density correlator $\phi_{q^*}^2(t)$ at the maximum of $I(q)$. We show two state points: one close to the repulsive glass and the other state close to the attractive one. Apart from an amplitude scaling factor, the dominant contribution is already sufficient to describe the long time behavior of $C_{\sigma\sigma}(t)$ for both attractive and repulsive glasses. However, for the

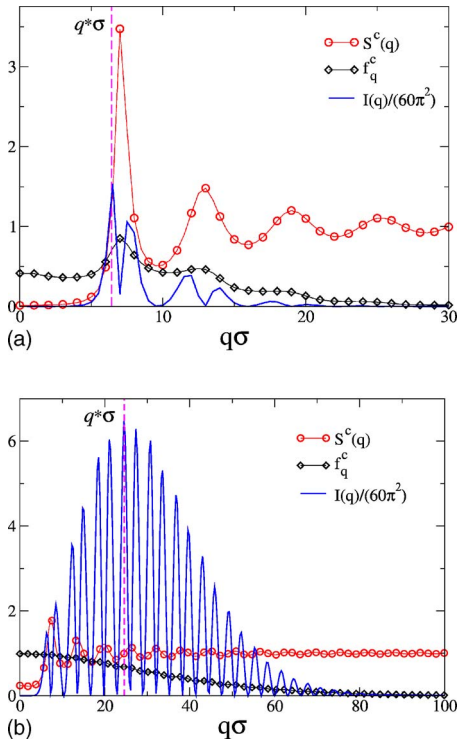

FIG. 6. Mode coupling contributions to the viscosity $I(q)/(60\pi^2)$, with $I(q)$ defined in Eq. (13). The wave vector at which $I(q)$ is maximum, $q^*\sigma$, is ≈ 6.5 for the repulsive glass (upper panel) and ≈ 24 for the attractive glass (lower panel). To compare, we report in the same figure also the q dependence of the critical nonergodicity parameter f_q^c and of the static structure factor $S^c(q)$.

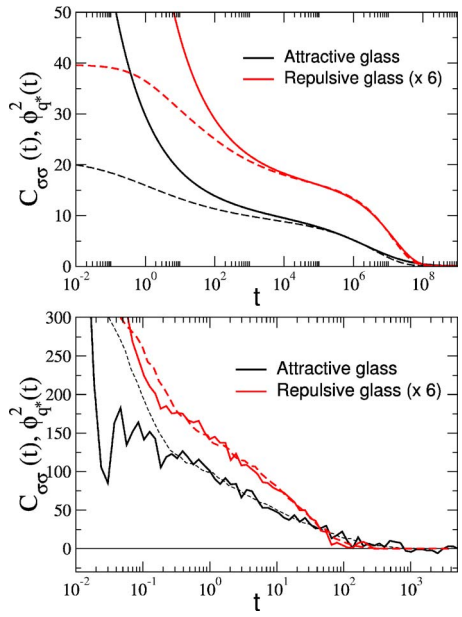

FIG. 7. Stress correlation function $C_{\sigma\sigma}(t)$ (full lines) for repulsive and attractive glasses calculated within MCT (top) and from simulations (bottom). The dashed lines are the squared density correlation functions $\phi^2_{q^*}(t)$, arbitrarily scaled in amplitude to overlap the long time behavior. For the MCT data, the wave vector q^* is the one reported in Fig. 6, while in the simulation panel it is the one which provides the best long time overlap between $\phi^2_{q^*}(t)$ and $C_{\sigma\sigma}(t)$.

attractive glass case, the decay of the squared density correlation shows a slightly smaller stretching as compared to $C_{\sigma\sigma}(t)$, which causes a small discrepancy at very long times. We attribute this difference to the fact that, in the case of attractive glasses, a large window of wave vectors contributes to the decay of the stress autocorrelation function (see Fig. 6).

In the lower panel of Fig. 7, the time dependencies of both $C_{\sigma\sigma}(t)$ and $\phi^2_{q^*}(t)$, as calculated from the simulation data, are also plotted. Here q^* is the wave vector at which the agreement between the time dependence of $C_{\sigma\sigma}(t)$ and $\phi^2_{q^*}(t)$ is optimal. The q^* values found in this way, respectively, $q^*\sigma \approx 7.5$ and $q^*\sigma \approx 26$, agree very well with those predicted by the theory.[40] Moreover, the behavior of $C_{\sigma\sigma}(t)$ is well described (within the numerical error) by a single squared density correlator for both glasses. The small discrepancy which was observed in the MCT data for the attractive glass is probably buried within the numerical noise.

Finally, we want to compare the elastic moduli for both glasses in the theoretical and numerical calculations. In order to calculate elastic and viscous moduli, the stress correlation functions calculated from simulations have to be Fourier transformed: $G(\omega)=i\omega\tilde{C}(\omega)$, where $\tilde{C}(\omega)$ is the Fourier transform of $C_{\sigma\sigma}(t)$. However, due to the noise in the correlation function, direct transformation produces very low quality results. Thus, we have fitted $C_{\sigma\sigma}(t)$ with empirical functional forms close to both glasses before performing the Fourier transform. We have chosen

$$C_{\sigma\sigma}(t) = C_{\sigma\sigma}(0)\{f(t/\tau_0) + A(1 - f(t/\tau_0))\exp\{-(t/\tau_1)^{\beta}\}\}, \tag{14}$$

where $f(x)$ is an even function that describes the short time relaxation of $C_{\sigma\sigma}(t)$: $f(x)=1/(1+x^2)$ for the repulsive glass (Fig. 2) and $f(x)=\exp\{-x^2\}$ for the attractive glass. τ_0 represents a microscopic time scale, which should be state independent, whereas τ_1 gives the time scale for the stress final relaxation. The parameter A gives the amplitude of the stored stress [so that $AC_{\sigma\sigma}(0)$ is the height of the plateau in $C_{\sigma\sigma}(t)$] and β is the stretching exponent, which according to the MCT prediction should be roughly equal to the stretching exponent of the density-density correlation function at q^*.

In Table III we present the parameters of the fittings for $C_{\sigma\sigma}(t)$ for states along path 1B, drawn in Fig. 2 as thin lines. As expected, τ_0 is state independent and τ_1 increases substantially when the glass transition is approached. A and β are correctly estimated only when the second relaxation is noticeable, i.e., above $\phi_c=0.55$; in these cases the amplitude is almost constant and β is compatible with the value obtained from the density correlation function at q^*, $\beta=0.52$.[38]

TABLE III. Parameters of the fitting of $C_{\sigma\sigma}(t)$ for states close to glass transition for soft-spheres (path 1B).

ϕ_c	$C_{\sigma\sigma}(0)$	A	τ_0	τ_1	β
0.58	181	0.18	0.024	13.30	0.509
0.57	156	0.16	0.026	3.56	0.665
0.55	134	0.15	0.024	1.18	0.759
0.53	83	0.23	0.025	0.20	0.421
0.50	34	0.39	0.024	0.03	0.353

TABLE IV. Parameters of the fitting of $C_{\sigma\sigma}(t)$ for states close to attractive glass transition (path 2).

ϕ_p	$C_{\sigma\sigma}(0)$	A	τ_0	τ_1	β
0.42	1650	0.077	0.011	81.48	0.325
0.41	1506	0.072	0.011	8.09	0.389
0.40	1470	0.061	0.011	3.49	0.585
0.39	1404	0.071	0.012	1.90	0.949
0.30	724	−0.085	0.013	0.07	1.757

The parameters of the fittings for the attractive glass (path 2) are given in Table IV. As before, τ_0 is almost constant, whereas τ_1 increases dramatically upon increasing the attraction strength.

From the values of the fits, we can directly compare other quantities between theory and simulations: namely, the $t=0$ value of the stress correlation function $C_{\sigma\sigma}(0)$ and the height of the long time plateau f_σ for both glasses. The results from MCT and simulations are reported in Table V for both studied paths. For both glasses, the simulations provide a lower value of $C_{\sigma\sigma}(0)$ and a larger value of f_σ with respect to MCT. Although numbers are not important *per se* when comparing to MCT, the ratio $f_\sigma/C_{\sigma\sigma}(0)$ is wrong by one order of magnitude for both attractive and repulsive glasses. This result seems to suggest that the factorization approximation[42] adopted to derive Eq. (12) may be too severe, although the structural relaxation is apparently well described, as shown by the comparisons of Fig. 7.

We finally directly compare the elastic and viscous moduli $G'(\omega)$ and $G''(\omega)$ in Fig. 8 for repulsive (top) and attractive glasses (bottom). We observe qualitatively the same trends for both transitions in theory and simulations, despite a shift in the absolute numbers.

(i) An increase of $G'(\omega)$ at large ω (but smaller than the microscopic frequency) with the approach to the glass transition.

(ii) The appearance of a minimum in G'' which moves to lower and lower ω with decreasing distance from the transition, in agreement with previous experimental and theoretical studies on both repulsive[50,51] and attractive glasses.[52,53] The minimum appears when $\epsilon \lesssim 0.01$ according to the theory ($\epsilon=|X_g-X|/X_g$, with X being either ϕ_c or Γ) and at slightly larger values of ϵ according to the simulations.

(iii) Much larger moduli (up to one order of magnitude) for the attractive than for the repulsive glass. This observation holds both for theory and simulations and agrees well with recent rheological measurements for thermoreversible sticky spheres.[19,54]

TABLE V. Approximate values of initial value of the stress correlation value $C_{\sigma\sigma}(0)$ and height of the plateau, f_σ for paths 1B and 2. The first two columns refer to simulation data and the last two to theoretical MCT predictions.

	$C_{\sigma\sigma}(0)$	f_σ	$C_{\sigma\sigma}^{\mathrm{MCT}}(0)$	f_σ^{MCT}
Path 1B	181	32	400	3
Path 2	1650	127	6000	100

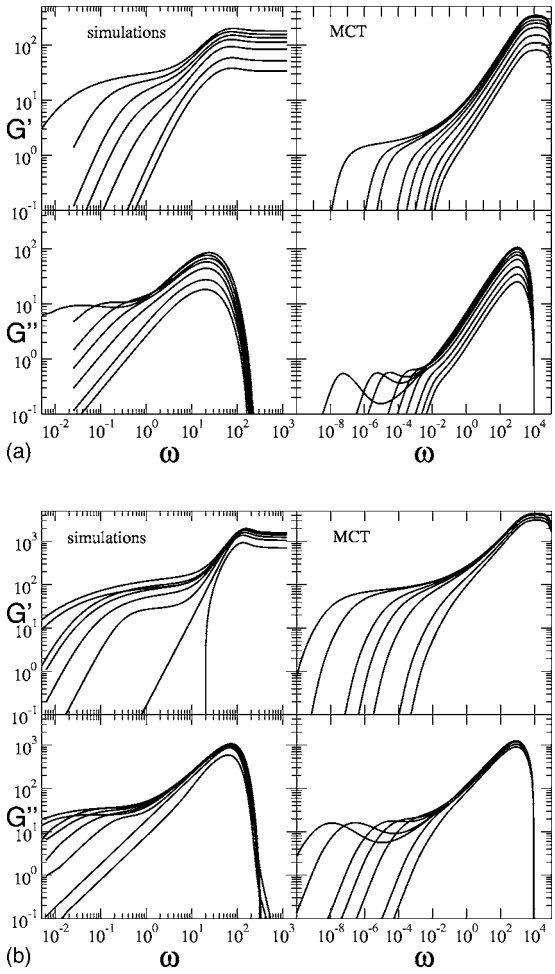

FIG. 8. Shear moduli G' and G'' from simulations (left) and MCT (right) for repulsive (top) and attractive glasses (bottom).

Overall, MCT correctly predicts the behavior of the viscoelastic properties on approaching both glass transitions. However, the results disagree again quantitatively, and more importantly in the ratio of the height of the plateau in G' (or minimum in G'') with respect to G'_∞ (or G''_{max}).

VI. BREAKDOWN OF STOKES-EINSTEIN RELATION

Finally, we discuss the breakdown of the Stokes-Einstein (SE) relation[55–61] close to the glass transition for all different studied paths.

We start by examining path I. Figure 9 shows the SE relation for the hard-sphere binary system and the soft sphere polydisperse system. To allow for a unifying picture, we plot the results as a function of the relative distance to the estimated glass transition ($\phi_c^G-\phi_c$). At low and moderate density, far from the transition the data are consistent with SE, although different value limits are obtained for model A or B; whereas the former takes the stick value, $D\eta/T=(3\pi\sigma)^{-1}$, the latter goes to the slip limit: $D\eta/T=(2\pi\sigma)^{-1}$. The reason for this difference is not clear,[62–64] but probably lies in the fine details of the interaction at short distances.[65,66] In both

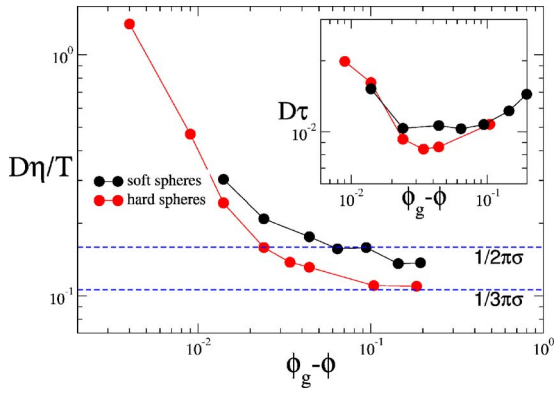

FIG. 9. Breakdown of the SE relation for $D\eta/T$ approaching the repulsive glass transition for paths 1A (empty red circles) and 1B (full black circles). For the hard-sphere case, $T=1$. The lines are guide to the eye. The two horizontal dashed lines mark the slip and stick values of the SE relation. Inset: $D\tau$ for the same paths.

cases, as the system approached the glass transition, the SE relation breaks down significantly, both in the form $D\eta$ and $D\tau$ (see inset).

Figure 10 shows the SE relation for the attractive glass case (path II) and along the reentrance (path III). The former case is rather clean and allows us to access a breakdown by two orders of magnitude with respect to the typical SE value, both in $D\eta/T$ and $D\tau$ (inset). For both paths, at large Γ (low T) a clear breakdown of both $D\tau$ and $D\eta/T$ is observed for the attractive glass.

For path III (reentrance case), one has to bear in mind that the path becomes parallel to the repulsive glass line at small Γ (see Fig. 1) and the increase is limited to the one observed in the HS case at the same packing. For this path we have also performed BD simulations. The BD results, also shown in Fig. 10, coincide with the MD data at all state points investigated, confirming that the SE behavior close to both repulsive and attractive glass transitions does not depend on the microscopic dynamics.

Data in Figs. 9 and 10 provide evidence that the breakdown of the SE is a phenomenon which can be observed in the vicinity of both the repulsive and the attractive glass

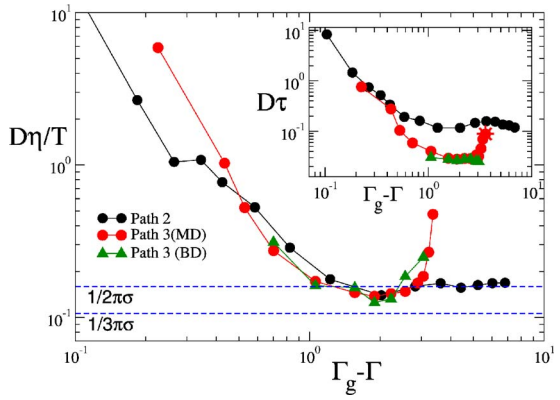

FIG. 10. Breakdown of the SE relation for $D\eta/T$ approaching the attractive glass transition for paths 2 (circles) and 3 (squares: MD and triangles: BD). Note the partial breakdown also at high T for the reentrant path due to the closeby repulsive glass. The two horizontal lines mark the slip and stick SE values. Inset: $D\tau$ for the same paths. The star indicates the HS value for path 3.

transitions. Within the investigated state window, it appears that the magnitude of the breakdown is enhanced in the attractive glass case, speaking for the presence of more intense dynamical heterogeneities[67–69] when confinement is originated by short-range bonds rather than by the excluded volume caging.

VII. CONCLUSIONS

In this article we reported the behavior of the viscosity in two models for short-range attractive colloids along three different paths in the attraction-strength packing-fraction plane. Along the first path, the system approaches the repulsive hard-sphere glass transition. Along the second path, it approaches the attractive glass. The third path is chosen in such a way that the system moves continuously from the repulsive to the attractive glass at constant packing fraction in the so-called reentrant region.[70] In this case, we have also compared Brownian and Newtonian simulation results, confirming that the viscosity is independent of the microscopic dynamics, in agreement with results based on the decay of density fluctuations in atomic liquids.[71]

We find that the increase of the viscosity on approaching the glass transition is consistent with a power-law divergence. The divergence of η can be described with the same exponent and critical packing fraction previously found for the collective relaxation time, but with an exponent different from the one that characterizes the divergence of the diffusion coefficient. This holds for both attractive and repulsive glasses.

As previously observed for diffusion and collective relaxations, the viscosity shows a nonmonotonic behavior with the attraction strength in the reentrant region (path III), confirming once more the validity of the theoretical MCT predictions.

To provide a connection between density relaxation and viscoelastic behavior we investigate the leading density fluctuation contributions to the decay of the stress autocorrelation function within MCT. Interestingly, for the case of the repulsive glass, it is possible to identify a small range of wave vectors (not far from the first peak of the structure factor) which are responsible for the viscoelastic behavior. In the case of the attractive glass, instead, the decay of the stress is associated with a much larger window of wave vectors, centered at much larger values. In this respect, the viscoelastic analysis confirms that dynamic arrest is driven by the short-lengh scale introduced by the bonding. We also compare the simulation results for the frequency dependence of the elastic moduli with corresponding theoretical MCT predictions, finding a substantial qualitative agreement.

Finally, we have evaluated the Stokes-Einstein relation. A clear breakdown of the relation is observed on approaching both glass lines, consistent with the different exponents characterizing the power-law dependence of diffusion and viscosity. The breakdown is particularly striking on approaching the attractive glass (a variation of the product $D\eta/T$ of up to two orders of magnitude in the investigated range). Recent theoretical work on MCT seems to provide insights that could be useful to reconcile the decoupling of

self-diffusion and viscosity (or relaxation time) within MCT.[58] It would be interesting in the future to deepen our knowledge of the connection between SE breakdown and the presence of dynamic heterogeneities, which has been previously studied for the same model.[67]

Note that while finalizing the manuscript, we become aware of a numerical study by Krekelberg *et al.*[72] which also reported the nonmonotonic behavior of the viscosity along the reentrant path and the breakdown of the SE relation. In that work, Krekelberg *et al.* seek a connection between the structural and dynamical properties of the system. We show here that MCT predicts correctly the properties of the system upon approaching the glass transitions, i.e., the connection between structure and dynamics is the nontrivial one provided by MCT.

ACKNOWLEDGMENTS

The authors thank M. Fuchs for stimulating discussions and S. Buldyrev for the MD code. The authors acknowledge support from MIUR-Prin and MRTN-CT-2003-504712. One of the authors (A.M.P.) was financially supported by the Spanish Ministerio de Educación y Ciencia (under Project No. MAT2006-13646-CO3-02).

[1] R. Mezzenga, P. Schurtenberger, A. Burbidge, and M. Michel, Nat. Mater. **4**, 729 (2005).
[2] R. P. Sear, Curr. Opin. Colloid Interface Sci. **11**, 35 (2006).
[3] V. Trappe and P. Sandkühler, Curr. Opin. Colloid Interface Sci. **8**, 494 (2004).
[4] L. Cipelletti and L. Ramos, J. Phys.: Condens. Matter **17**, 253 (2005).
[5] F. Sciortino and P. Tartaglia, Adv. Phys. **54**, 471 (2005).
[6] E. Zaccarelli, J. Phys.: Condens. Matter **19**, 323101 (2007).
[7] A. Yethiraj and A. V. Blaaderen, Nature (London) **421**, 513 (2003).
[8] V. Prasad, D. Semwogerere, and E. R. Weeks, J. Phys.: Condens. Matter **19**, 3102 (2007).
[9] L. Fabbian, W. Götze, F. Sciortino, P. Tartaglia, and F. Thiery, Phys. Rev. E **59**, 1347 (1999).
[10] J. Bergenholtz and M. Fuchs, J. Phys.: Condens. Matter **11**, 10171 (1999).
[11] K. A. Dawson, G. Foffi, M. Fuchs, W. Götze, F. Sciortino, M. Sperl, P. Tartaglia, T. Voigtmann, and E. Zaccarelli, Phys. Rev. E **63**, 011401 (2001).
[12] W. Götze and M. Sperl, Phys. Rev. E **66**, 011405 (2002).
[13] M. Sperl, Phys. Rev. E **68**, 031405 (2003).
[14] K. N. Pham, A. M. Puertas, J. Bergenholtz, S. U. Egelhaaf, A. Moussaïd, P. N. Pusey, A. B. Schofield, M. E. Cates, M. Fuchs, and W. C. K. Poon, Science **296**, 104 (2002).
[15] T. Eckert and E. Bartsch, Phys. Rev. Lett. **89**, 125701 (2002).
[16] S. H. Chen, W.-R. Chen, and F. Mallamace, Science **300**, 619 (2003).
[17] K. N. Pham, S. U. Egelhaaf, P. N. Pusey, and W. C. K. Poon, Phys. Rev. E **69**, 011503 (2004).
[18] J. Grandjean and A. Mourchid, Europhys. Lett. **65**, 712 (2004).
[19] T. Narayanan, M. Sztucki, G. Belina, and F. Pignon, Phys. Rev. Lett. **96**, 258301 (2006).
[20] W. Götze, *Liquids, Freezing and the Glass Transition* (North-Holland, Amsterdam, 1991), pp. 287–503.
[21] A. M. Puertas, M. Fuchs, and M. E. Cates, Phys. Rev. Lett. **88**, 098301 (2002).
[22] G. Foffi, K. A. Dawson, S. V. Buldrey, F. Sciortino, E. Zaccarelli, and P. Tartaglia, Phys. Rev. E **65**, 050802 (2002).
[23] E. Zaccarelli, G. Foffi, K. A. Dawson, S. V. Buldrey, F. Sciortino, and P. Tartaglia, Phys. Rev. E **66**, 041402 (2002).
[24] A. Puertas, M. Fuchs, and M. E. Cates, Phys. Rev. E **67**, 031406 (2003).
[25] Z. Cheng, J. Zhu, P. Chaikin, S.-E. Phan, and W. Russel, Phys. Rev. E **65**, 041405 (2002).
[26] M. Fuchs and M. E. Cates, Faraday Discuss. **123**, 267 (2003).
[27] S. Shah, Y.-L. Chen, K. Schweizer, and C. Zukoski, J. Chem. Phys. **119**, 8747 (2003).
[28] E. Zaccarelli, F. Sciortino, S. V. Buldyrev, and P. Tartaglia, *Short-Ranged Attractive Colloids: What is the Gel State*? (Elsevier, Amsterdam, 2004), pp. 181–194.
[29] M. G. Noro and D. Frenkel, J. Chem. Phys. **113**, 2941 (2000).
[30] M. A. Miller and D. Frenkel, J. Chem. Phys. **121**, 535 (2004).
[31] F. Sciortino, P. Tartaglia, and E. Zaccarelli, Phys. Rev. Lett. **91**, 268301 (2003).
[32] D. C. Rapaport, *The Art of Molecular Dynamic Simulation* (Cambridge University Press, Cambridge, U.K., 1995).
[33] G. Foffi, C. D. De Michele, F. Sciortino, and P. Tartaglia, Phys. Rev. Lett. **94**, 078301 (2005).
[34] A. Scala, T. Voigtmann, and C. De Michele, J. Chem. Phys. **126**, 134109 (2007).
[35] A. M. Puertas, M. Fuchs, and M. E. Cates, Phys. Rev. E **67**, 031406 (2003).
[36] B. Alder, D. Gass, and T. Wainwright, J. Chem. Phys. **53**, 3813 (1970).
[37] J. R. Melrose, Europhys. Lett. **19**, 51 (1992).
[38] T. Voigtmann, A. M. Puertas, and M. Fuchs, Phys. Rev. E **70**, 061506 (2004).
[39] A. M. Puertas, M. Fuchs, and M. E. Cates, J. Phys. Chem. B **109**, 6666 (2005).
[40] A. M. Puertas, E. Zaccarelli, and F. Sciortino, J. Phys.: Condens. Matter **17**, L271 (2005).
[41] O. Henrich, A. M. Puertas, M. Sperl, J. Baschnagel, and M. Fuchs, e-print arXiv:cond-mat/07050637
[42] G. Nägele and J. Bergenholtz, J. Chem. Phys. **108**, 9893 (1998).
[43] S. Asakura and F. Oosawa, J. Polym. Sci. **33**, 183 (1958).
[44] M. Dijkstra, J. M. Brader, and R. Evans, J. Phys.: Condens. Matter **11**, 10079 (1999).
[45] M. Dijkstra, R. van Roij, and R. Evans, J. Chem. Phys. **113**, 4799 (2000).
[46] M. Schmidt, H. Löwen, J. M. Brader, and R. Evans, Phys. Rev. Lett. **85**, 1934 (2000).
[47] M. Schmidt, H. Löwen, J. M. Brader, and R. Evans, J. Phys.: Condens. Matter **14**, 9353 (2002).
[48] E. Zaccarelli, H. Löwen, P. P. F. Wessels, F. Sciortino, P. Tartaglia, and C. N. Likos, Phys. Rev. Lett. **92**, 225703 (2004).
[49] M. Fuchs, W. Gotze, I. Hofacker, and A. Latz, J. Phys.: Condens. Matter **3**, 5047 (1991).
[50] T. G. Mason and D. A. Weitz, Phys. Rev. Lett. **75**, 2770 (1995).
[51] M. Fuchs and M. R. Mayr, Phys. Rev. E **60**, 5742 (1999).
[52] K. A. Dawson, G. Foffi, F. Sciortino, P. Tartaglia, and E. Zaccarelli, J. Phys.: Condens. Matter **13**, 9113 (2001).
[53] F. Mallamace, P. Tartaglia, W. R. Chen, A. Faraone, and S. Hsin Chen, J. Phys.: Condens. Matter **16**, 4975 (2004).
[54] M. Sztucki, T. Narayanan, G. Belina, A. Moussaïd, F. Pignon, and H. Hoekstra, Phys. Rev. E **74**, 051504 (2006).
[55] F. H. Stillinger and J. A. Hodgdon, Phys. Rev. E **50**, 2064 (1994).
[56] M. D. Ediger, Annu. Rev. Phys. Chem. **51**, 99 (2000).
[57] S. K. Kumar, G. Szamel, and J. F. Douglas, J. Chem. Phys. **124**, 4501 (2006).
[58] G. Biroli and J.-P. Bouchaud, J. Phys.: Condens. Matter **19**, 5101 (2007).
[59] Y. Jung, J. P. Garrahan, and D. Chandler, Phys. Rev. E **69**, 061205 (2004).
[60] Y. Brumer and D. R. Reichman, Phys. Rev. E **69**, 041202 (2004).
[61] S. R. Becker, P. H. Poole, and F. W. Starr, Phys. Rev. Lett. **97**, 055901 (2006).
[62] P. Segré, S. Meeker, P. Pusey, and W. Poon, Phys. Rev. Lett. **75**, 958 (1995).
[63] C. D. Michele and D. Leporini, Phys. Rev. E **63**, 036701 (2001).
[64] A. Moreno, S. Buldyrev, E. L. Nave, I. Saika-Voivod, F. Sciortino, P. Tartaglia, and E. Zaccarelli, Phys. Rev. Lett. **95**, 157802 (2005).
[65] R. Biswas, S. Bhattacharyya, and B. Bagchi, J. Phys. Chem. B **102**, 3252 (1998).
[66] B. Bagchi and S. Bhattacharyya, Adv. Chem. Phys. **116**, 67 (2001).
[67] A. Puertas, M. Fuchs, and M. E. Cates, J. Chem. Phys. **121**, 2813 (2004).
[68] C. J. Dibble, M. Kogan, and M. J. Solomon, Phys. Rev. E **74**, 041403 (2006).
[69] Y. Gao and M. L. Kilfoil, Phys. Rev. Lett. **99**, 078301 (2007).
[70] F. Sciortino, Nat. Mater. **1**, 145 (2002).
[71] T. Gleim, W. Kob, and K. Binder, Phys. Rev. Lett. **81**, 4404 (1998).
[72] W. P. Krekelberg, J. Mittal, V. Ganesan, and T. M. Truskett, J. Chem. Phys. **127**, 044502 (2007).